Bio-Design and Manufacturing (2022) 5:294–304
https://doi.org/10.1007/s42242-021-00175-y

RESEARCH ARTICLE

4D printing of core–shell hydrogel capsules for smart controlled drug release

Shuo Zu[1] · Zhihui Zhang[1] · Qingping Liu[1] · Zhenguo Wang[1] · Zhengyi Song[1] · Yunting Guo[1] · Yuanzhu Xin[2] · Shuang Zhang[1]

Received: 26 July 2021 / Accepted: 14 November 2021 / Published online: 21 February 2022

Abstract

Personalized drugs, as well as disease-specific and condition-dependent drug release, have been highly desired in drug delivery systems for effective and safe therapies. Four-dimensional (4D) printing, as a newly emerging technique to develop drug capsules, displays unique advantages that can autonomously control drug release according to the actual physiological circumstances. Herein, core–shell structured hydrogel capsules were developed using a multimaterial extrusion-based 4D printing method, which consists of a model drug as the core and UV cross-linked poly(*N*-isopropylacrylamide) (PNIPAM) hydrogel as the shell. Owing to the lower critical solution temperature (LCST)-induced shrinking/swelling properties, the prepared PNIPAM hydrogel capsules showed temperature-responsive drug release along with the topography changes in the cross-linked PNIPAM network. The in vitro drug release test confirmed that the PNIPAM hydrogel capsules can autonomously control their drug release behaviors according to changes in ambient temperature. Moreover, the increased shell thickness of these capsules causes an obvious reduction in drug release rate, distinctly indicating that the drug release behavior can be well adjusted by setting the shell thickness of the capsules. The proposed 4D printing strategy pioneers the paradigm of smart drug release by showing great potential in the smart controlled release of drugs and macromolecular active agents.

Graphic abstract

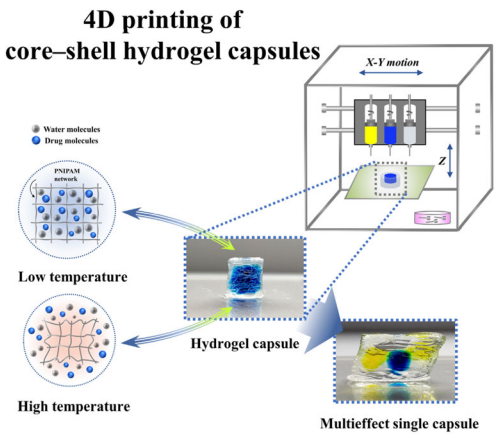

Keywords 4D printing · Hydrogel capsules · Controlled release · Poly(*N*-isopropylacrylamide) (PNIPAM) · Personalized drugs

✉ Zhihui Zhang
zhzh@jlu.edu.cn

✉ Qingping Liu
liuqp@jlu.edu.cn

[1] Key Laboratory of Bionic Engineering, Ministry of Education, Jilin University, Changchun 130025, China

[2] School of Mechanical and Aerospace Engineering, Jilin University, Changchun 130025, China

Introduction

Traditional dosage forms for oral drug delivery are mainly tablets and two-piece capsules, with the major issues being a fixed dose and limited dosage strength of drugs [1]. However, for the treatment of a given type of disease, the individual needs of each patient may be different [2, 3]. The increasing demand for personalized drugs (in terms of dosage strength, release time, and/or drug combinations) [4, 5] by specific individuals is changing the landscape of drug manufacturing, urging the drug industry to consider new methods of drug production [1, 6–9].

3D printing (3DP) is a computer-aided manufacturing process that assembles materials into parts via layer-by-layer deposition or solidification processes [10]. The 3DP approach offers various advantages suited to meeting the challenges facing the drug sector, including rapid prototyping, multimaterial integration, the fabrication of complex geometries [11], and the possibility of using a wide range of excipients to solubilize [12], target, or control drug release [13]. To date, several methods have been leveraged to fabricate personalized drugs, such as fused deposition modeling (FDM) [14–17], stereolithography (SLA) [1, 18, 19], extrusion printing [20, 21], selective laser sintering (SLS) [22] and inkjet printing [13, 23, 24] 3DP processes. Among them, the extrusion 3D printing process has the advantages of easily adjusted printing conditions, low machine operating cost, simplicity, and convenient customization [25–27]. Moreover, it can be used to print biopolymer materials carrying living cells [28]. In contrast, 4D printing, as an emerging technique originating from 3D printing where the material shape, properties, and functionality are able to transform under external stimuli, shows promising capabilities and has broad potential applications [25, 29]. Smart materials that can transform their morphologies in response to external stimuli, such as hydrogels, shape memory materials, and liquid crystalline elastomers, are widely applied in 4D printing technologies [30, 31].

Hydrogels are three-dimensional, cross-linked networks of water-soluble polymers [32], offering an environment similar to that of natural tissues [33]. Owing to their high elasticity, softness, and biocompatibility [34], hydrogels have been applied in various medical fields, such as cellular immobilization [35], bioengineering, and regenerative medicine [36–38]. The unique physical properties of hydrogels have sparked particular interest in their utility in drug delivery systems [39–41]. Since the traditional manufacturing processes of hydrogel drugs can produce 2D forms or simple 3D structures by templating, the number of hydrogel drugs produced by 3DP is gradually increasing. However, challenges still remain in the application of the current 3DP hydrogel drugs, such as: only a single type of drug can be loaded [1, 42]; printed hydrogel drugs have poor shape fidelity [43, 44]; sometimes the hydrogel must be soaked in the drug solution to load the drug [39]; and the release modes of drugs are mostly delayed, immediate and/or constant release [45], which cannot be controlled in real time by environmental stimuli and do not fully utilize the advantages of 3DP hydrogel drugs [46].

In this paper, we propose multimaterial extrusion-based 4D printed hydrogel capsules for smart controlled drug release. The 4D-printed capsules have a core–shell structure, where the "core" is composed of a model drug, and the "shell" is composed of poly(*N*-isopropylacrylamide) (PNIPAM) hydrogel cross-linked by UV irradiation [47–49]. PNIPAM is a representative thermosensitive polymer that displays a lower critical solution temperature (LCST) phase transition in water, and it undergoes a rapid hydrophilic-hydrophobic transition at approximately 32 °C [50]. Due to its thermo-responsive characteristics, the PNIPAM hydrogel demonstrates LCST-induced shrinking/swelling properties, which can cause the changed topography of the cross-linked PNIPAM network. The temperature sensitivity of PNIPAM hydrogel was explored by measuring the swelling ratio (SR) of the hydrogel at different temperatures. Moreover, the effects of hydrogel capsule shell thickness and environmental temperature on drug release properties were investigated. Finally, the in vitro drug release profiles of the hydrogel capsules were analyzed to explore the self-controlled drug release behavior based on the environmental conditions.

Experimental section

Materials

The monomer *N*-isopropylacrylamide (NIPAM, 2% stabilizer), the photoinitiator α-ketoglutaric acid, the cross-linker *N*,*N*′-methylenebisacrylamide (MBAA), the rheology modifier Carbomer 940, and NaOH were all purchased from Shanghai Macklin Biochemical Co., Ltd. (China). The model drugs Brilliant Blue and Lemon Yellow were obtained from Tianjin Duofuyuan Industrial Co., Ltd. (China). The phosphate-buffered solution (PBS) was purchased from Shanghai Ruichu Biotech Co., Ltd. (China). All materials were used as received, and all solutions were prepared using ultrapure water (resistivity = 18.2 MΩ·cm).

Preparation of printing inks

We prepared the NIPAM printing ink according to a previous report [51]. First, NIPAM was dissolved in water to form a 2 mol/L solution. Then, Carbomer 940 powder (1.0, 3.0, and 5.0% (w/v)) was added to 10 mL of 2 mol/L NIPAM. Two hundred microliters of 0.1 mol/L α-ketoglutaric acid and 40 μL of 0.1 mol/L MBAA were added to the precursor

ink, followed by mixing using a planetary centrifugal mixer (Thinky, AR-100). As the carbomer swelled to a different extent at different pH values, 70 μL of 10 mol/L NaOH was used to adjust the pH level, and the NIPAM printing ink was mixed again and degassed for 5 min.

To prepare printing inks containing the model drugs, Carbomer 940 powder (1.0% (w/v)) and 0.05 g of model drug (Brilliant Blue and Lemon Yellow) were added to 10 mL of water, followed by mixing using a Thinky mixer. After adjusting the pH level, the inks were mixed again and degassed for 5 min.

Subsequently, all of the inks were loaded into syringes for later use. Before the syringes were assembled on the 3D printer, the inks were degassed again to ensure that there were no bubbles affecting the subsequent printing performance.

Measurement of rheological properties

The rheological properties of NIPAM printing inks with different carbomer concentrations were measured by a rheometer (MCR702, Anton-Paar) with a 25 mm diameter plate at 25 °C. To quantitatively determine the storage modulus (G') and loss modulus (G'') as a function of oscillation stress, dynamic oscillation stress sweep experiments were carried out within shear stresses from 1 to 1000 Pa at a frequency of 1 Hz. To explore the viscosity of NIPAM printing inks at different carbomer concentrations, a steady-state flow experiment was carried out with shear rates ranging from 0.01 to 1000 s^{-1}.

4D printing

The samples were printed by a homemade extrusion 3D printer with freely designable printing parameters. Syringes with 0.34 mm inner nozzle diameter were used to load the printing inks and extrude strands. The syringes were assembled on the 3D printer. In the extrusion process, the extrusion pressure changed with the printing speed and nozzle diameter. Open-source slicing software (Slic3r) was employed to regulate the parameters. The 3D printing process was performed under ambient conditions. The printed samples were placed in an airtight box from which oxygen was expelled by constant nitrogen flux, and then exposed to UV light (365 nm) for 40 min to fix their shape.

Microstructure of PNIPAM hydrogels at different temperatures

The internal microstructure of PNIPAM hydrogels at different temperatures was observed through a scanning electron microscope (Model Evo18 Carl Zeiss, Oberkochen, Germany). Samples of the hydrogels were lyophilized in a freeze-drying oven (LGJ-10C, Beijing Four Ring Scientific Instrument Factory Co., Ltd., China) for 48 h and coated with gold before scanning electron microscopy (SEM) examination. Two distinct treatment methods were adopted for different hydrogel samples before lyophilization. In the first method, when the swollen hydrogel samples reached the equilibrium swelling state in water at different temperatures, they were frozen thoroughly at − 50 °C for 24 h and then lyophilized. In the other method, when the swollen hydrogel samples reached the equilibrium swelling state in water at different temperatures, they were immediately frozen in liquid nitrogen and then lyophilized.

Macroscopic morphology of PNIPAM hydrogels at different temperatures

The macroscopic morphology of PNIPAM hydrogels at different temperatures was observed through a digital microscope (VHX-6000, KEYENCE). Before the observations, the swollen hydrogel sheet samples reached the equilibrium swelling state in water at room temperature. An infrared camera (FLIR E8, USA) was used to measure the temperature variations in the hydrogel sheet samples, and temperature data were obtained from the surface of the hydrogel and heating plate.

Determination of swelling ratio (SR)

The PNIPAM hydrogels were blotted with filter paper to remove any uncured liquid formulation on the surface immediately after UV curing, and they were weighed (W_i). Subsequently, the hydrogels were placed in water at different temperatures for 12 h. The weight of the hydrogels was recorded at regular time intervals (W_t), and any excess water was carefully wiped off before weighing the samples. After the testing was finished, the hydrogels were dried and weighed (W_d). SR was calculated using the following equation: $SR = W_t/W_i$. The water content of PNIPAM hydrogel after UV curing was calculated using the following equation: water content $(\%) = (1 - W_d/W_i) \times 100\%$.

In vitro drug release

In order to investigate the controlled release properties of the hydrogel capsules, we explored the drug release parameters of the capsules with a shell thickness of 2 mm at different temperatures and different shell thicknesses (2, 4, and 6 mm) at 22 °C. The hydrogel capsules were placed into vials containing 40 mL of PBS (pH = 7.4) at different temperatures. Then, 50 μL of the release medium was removed at each predetermined time point. The amount of Brilliant Blue released was measured by a UV–Vis spectrophotometer (Evolution

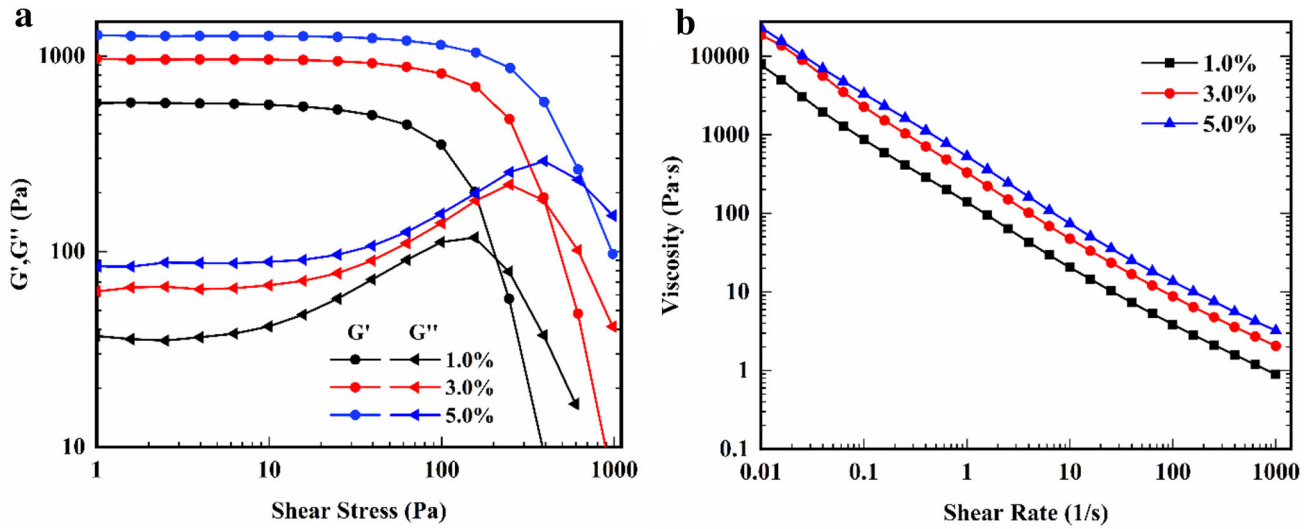

Fig. 1 Rheological properties of NIPAM printing inks. **a** Log–log plot of shear storage modulus (G') and shear loss modulus (G'') as a function of shear stress for NIPAM printing inks with varying carbomer concentrations. **b** Log–log plot of viscosity as a function of shear rate for NIPAM printing inks with varying carbomer concentrations

350, Thermo Fisher Scientific (China) Co., Ltd.). All capsule release experiments were carried out in triplicate.

Results and discussion

Rheological properties of the printing inks

The smart hydrogel capsules were printed by an extrusion 3D printer, and the rheological properties of the printing ink affected the quality of the prints. We used carbomer as the rheological modifier; therefore, it was necessary to first determine the concentration of carbomer. The rheological behaviors of NIPAM printing inks with different carbomer concentrations are shown in Fig. 1a. It can be seen that, at the initial section of the curves, the shear storage modulus G' of the inks is larger than the shear loss modulus G'', indicating that the inks are in a stable gel state with excellent elasticity. When the shear stress is larger than a certain value, the shear loss modulus G'' exceeds the shear storage modulus G', indicating the liquid state of the printing inks. The shear storage modulus G' and the shear loss modulus G'' increase with the concentration of carbomer. The viscosity of NIPAM printing ink is also a crucial factor for 3D printing. Figure 1b describes the viscosity as a function of the shear rate. The viscosity value increased from 7757.6 to 23,269 Pa·s under a low shear rate (10^{-2} s^{-1}), and it increased from 0.89 to 3.21 Pa·s under a high shear rate (10^{3} s^{-1}). The inks clearly show shear-thinning behavior, and the ink with higher carbomer concentration has higher viscosity. We further compared the extrusion fluency of inks with different carbomer concentrations (Fig. S1, Supplementary Information). We found that 5% (w/v) carbomer was too much to be uniformly dispersed in the printing inks, which led to the nozzle easily clogging during printing. The ink with 3% (w/v) carbomer required a prolonged time or a greater extrusion pressure to extrude the ink due to its high viscosity. In contrast, the inks with 1% (w/v) carbomer showed excellent performance under the same printing parameters, and the printed shape also exhibited high fidelity [51]. Moreover, less rheology modifiers in the ink will increase the water content of the hydrogel and better maintain its original properties, promoting the diffusion of drugs and nutrients [52]. Therefore, we used inks with 1% (w/v) carbomer for printing.

Multimaterial extrusion 4D printing

Figure 2a displays the schematic diagram of the homemade multimaterial extrusion 3D printer, whose printing parameters can be freely designed. Figure 2b provides a schematic illustration of the 4D-printed hydrogel capsules with a core–shell structure. The "core" is composed of the model drug, and the "shell" is composed of PNIPAM hydrogel. Figure 2c shows the shape of a printed hydrogel capsule with a shell thickness of 2 mm before and after UV irradiation. The hydrogel capsule was cross-linked by UV irradiation. First, the photoinitiator α-ketoglutaric acid was activated into radicals by 365 nm UV light and then interacted with the monomer NIPAM and cross-linker MBAA to form PNIPAM hydrogels [47, 49, 50]. The printed shape exhibits high fidelity, and the capsule is able to retain its shape until

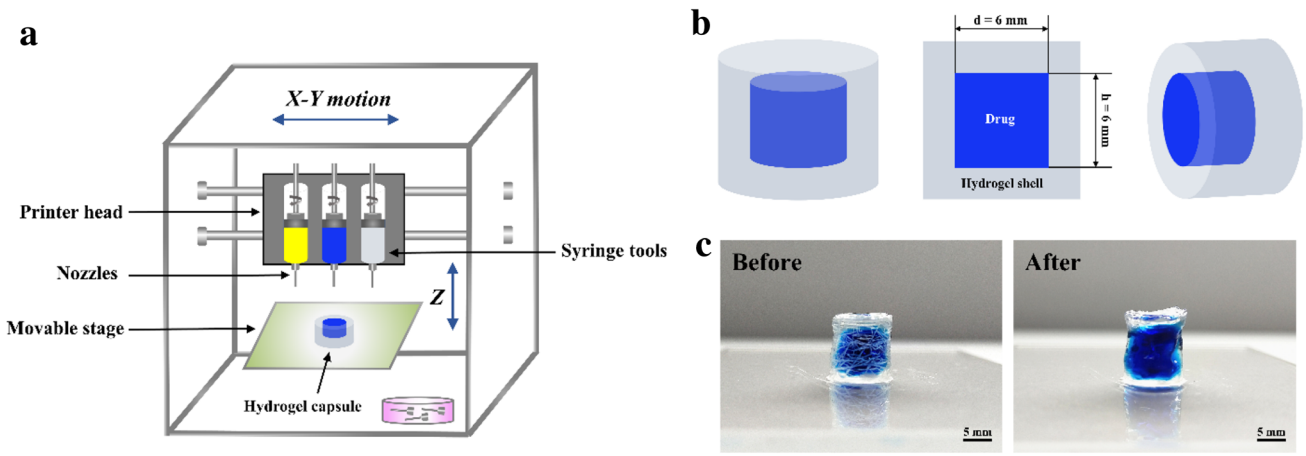

Fig. 2 4D printing of hydrogel capsules. **a** Schematic diagram of the homemade extrusion 3D printer. **b** Left–right schematic of the 4D-printed hydrogel capsules, including the overall structure of core–shell, longitudinal section, and transverse section. **c** Sample photographs of 4D-printed hydrogel capsules with a shell thickness of 2 mm before (left) and after (right) UV curing

fully UV cross-linked, as required. The structure and shape of the capsules were close to the predesigned conditions.

Characterization of PNIPAM hydrogel

Influence of temperature on the microstructure

Figure 3 exhibits SEM photographs of the internal microstructure of freeze-dried hydrogel samples. It is worth noting that, to more accurately observe the relative pore size of PNIPAM hydrogel at different temperatures, two distinct treatment methods were adopted for different hydrogel samples before lyophilization. Figures 3a and 3b show the internal microstructure of 22 °C and 42 °C hydrogel samples that were both thoroughly frozen at − 50 °C for 24 h before lyophilization, respectively. Figures 3c and 3d show the internal microstructure of 22 °C and 42 °C hydrogel samples that were both immediately frozen in liquid nitrogen before lyophilization, respectively. As seen in Fig. 3, the PNIPAM hydrogels presented a honeycomb-like structure and uniform distribution. Due to the influence of lyophilization process conditions, varied pore sizes were observed on the hydrogels treated by the two different methods but under the same temperature. The hydrogels at 42 °C (Figs. 3b and 3d) exhibited a denser microstructure than those at 22 °C (Figs. 3a and 3c). As the temperature increased, the internal pore size of the hydrogel reduced, indicating that the hydrogel has different pore sizes at different temperatures and exhibits good temperature sensitivity.

Influence of temperature on macroscopic morphology

Figures 4a and 4d show the infrared images of hydrogels taken by an infrared camera, where the real-time temperature distribution of the PNIPAM hydrogel sheet samples is clearly shown. Figures 4b and 4e are the enlarged views indicated by the crosshairs in Figs. 4a and 4d, respectively. Figures 4c and 4f display the 3D morphology images of Figs. 4b and 4e, respectively. Figures 4b and 4e show the surface macroscopic morphology of the hydrogels at approximately 23 °C and 36.3 °C, respectively. As seen, "sweat" appears on the hydrogel surface with increasing temperature (Fig. 4e), and the morphology of the hydrogel with "sweat" is more directly reflected by the 3D composite image (Fig. 4f). Moreover, the overall size of the hydrogel sheet sample gradually decreases, and the volume shrinks with increasing temperature (Movie S1, Supplementary Information). These volume changes can be attributed to the alteration of polymer hydration state with the temperature change. Temperature variations can affect the hydrophobic interactions between groups and the hydrogen bonding between macromolecular chains. In aqueous media at approximately 32 °C, PNIPAM undergoes a rapid hydrophilic-hydrophobic transition, and this temperature is termed LCST [50, 53]. When the temperature is lower than LCST, the polymer molecular chain is stretched, and the water molecules are dispersed in the network structure. Meanwhile, when the temperature rises above LCST, the interactions between the polymer chain segments increase, and the network structure shrinks. As a result, water molecules are squeezed out, resulting in a volume decrease, which leads to the phenomenon of "sweating." The above observations indicate that the PNIPAM hydrogel has high sensitivity to temperature.

Temperature sensitivity of PNIPAM hydrogel

The thermal sensitivity of PNIPAM hydrogel was determined by measuring the SR of the hydrogel at different

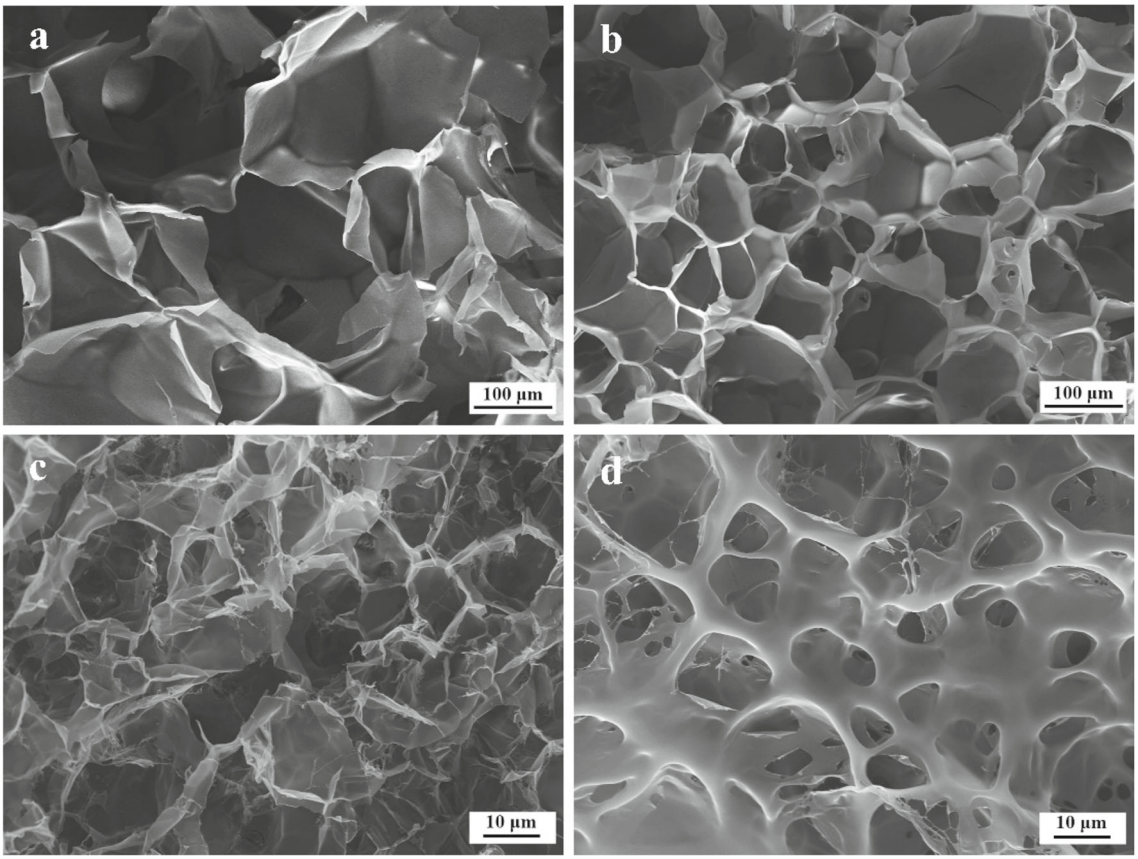

Fig. 3 SEM photographs of PNIPAM hydrogels. The internal microstructure of **a** 22 °C and **b** 42 °C hydrogel samples that were thoroughly frozen at − 50 °C for 24 h before lyophilization, and the internal microstructure of **c** 22 °C and **d** 42 °C hydrogel samples that were immediately frozen in liquid nitrogen before lyophilization

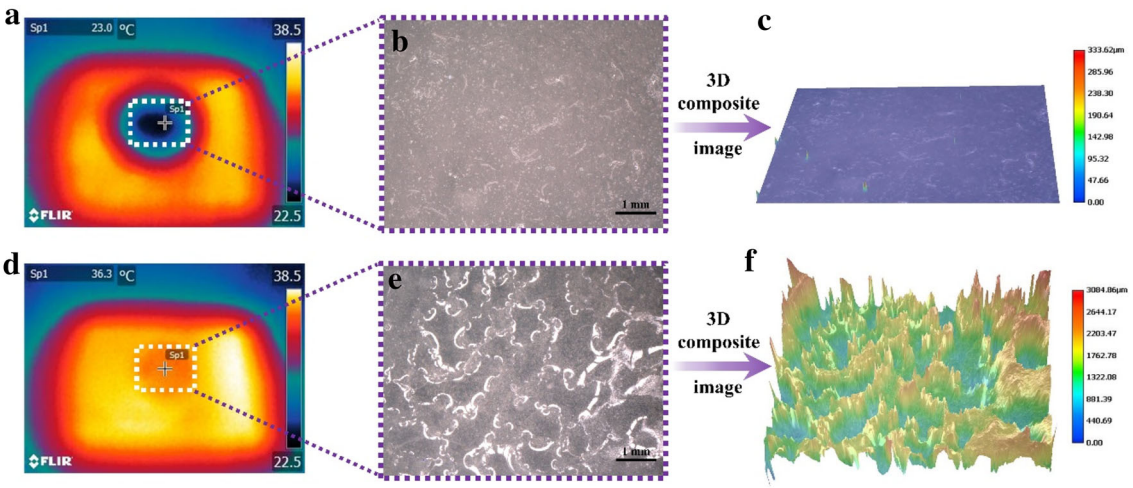

Fig. 4 Macroscopic morphology of PNIPAM hydrogels at different temperatures. **a**, **d** Real-time temperature distribution of hydrogels. **b** Surface macroscopic morphology of hydrogel at approximately 23 °C. **c**, **f** Morphological 3D composite images of hydrogels. **e** Surface macroscopic morphology of hydrogel at approximately 36.3 °C

temperatures. Body temperature is one of the major physiological parameters related to health state [54]. Normally, the body temperature varies from 35 to 42 °C, and values lower than 35 °C are considered as hypothermia [55]. In aqueous media at approximately 32 °C, PNIPAM undergoes a rapid hydrophilic-hydrophobic transition. To better evaluate the temperature sensitivity of the PNIPAM hydrogel above and below its LCST, the hydrogel was assessed over a wide temperature range, including the body temperature window. Figure 5 illustrates the influence of temperature on the SR of PNIPAM hydrogel. PNIPAM hydrogels at lower temperatures had a higher SR than those at higher temperatures, while the hydrogels at higher temperatures reached an equilibrium swelling state earlier than those at lower temperatures. When PNIPAM hydrogel is kept at a lower temperature, internal hydrogen bonds between amide groups and water molecules become dominant, thus facilitating the swelling of the PNIPAM network in water [39, 56]. However, the hydrophobic interactions between hydrophobic segments surge as the temperature increases, weakening the hydrogen bonds between amide groups and water molecules, resulting in hydrogel shrinking [50, 56, 57]. As a result, the water molecules are squeezed out, leading to a decrease in the hydrogel volume. Therefore, hydrogels at higher temperatures had a lower SR, and they reached an equilibrium swelling state earlier than those at lower temperatures. Since the average water content of the UV-cured PNIPAM hydrogel was 76%, the hydrogel at 42 °C—much higher than LCST—shows deswelling at the beginning of the curve, as shown in Fig. 5. It is seen in the figure that PNIPAM hydrogel has excellent temperature sensitivity, and its internal pore size can change with temperature. The pore size is approximately constant at a certain temperature when the hydrogel reaches the equilibrium swelling state. These properties lay the foundation for achieving a smart controlled drug release from 4D-printed hydrogel capsules under different temperature stimuli.

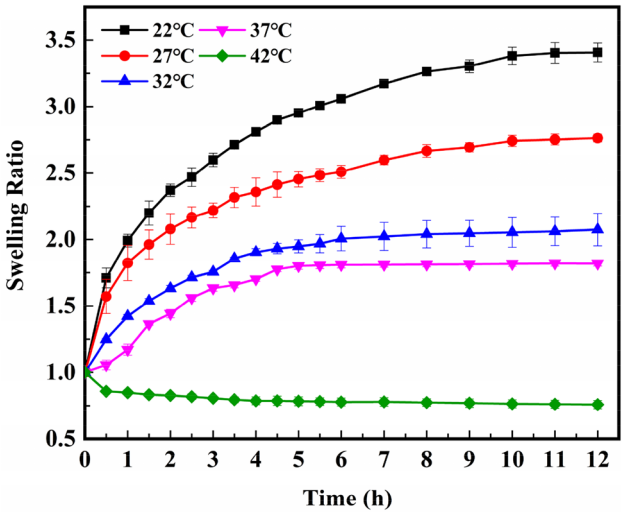

Fig. 5 Influence of temperature on the SR of PNIPAM hydrogel

In vitro drug release profiles

Effect of temperature on drug release

The hydrogel capsules have a core–shell structure, where the "core" is composed of the model drug Brilliant Blue, and the "shell" is composed of PNIPAM hydrogel. Figure 6a shows the schematic diagram of the temperature-dependent release of PNIPAM hydrogel shell. Regular PNIPAM hydrogels containing drugs shrink rapidly at high temperatures, resulting in a rapid and uncontrollable drug release [39, 57]. In contrast, the core–shell hydrogel capsules featuring PNIPAM hydrogel as the capsule shell exhibit the advantage of self-controlled drug release behavior according to ambient temperature. Normally, the body temperature varies from 35 to 42 °C, while patients with hypothermia have body temperatures below 35 °C [55]. As shown in Fig. 6b, experiments on drug release from hydrogel capsules with a shell thickness of 2 mm were conducted over a wide temperature range, including the body temperature window. After 12 h, more than 80% of the Brilliant Blue was released from the hydrogel capsules at the relatively low temperatures of 22 °C and 27 °C, while the proportions of drug released at 32 °C, 37 °C, and 42 °C were approximately 77%, 68%, and 60%, respectively. These experimental results indicate that high temperature triggers a relatively low drug release behavior. Drug release is highly dependent on the contact between the drug and the release media in the hydrogel shell. The mesh size regulates steric interactions between the drug and the hydrogel network [58, 59]. The larger the size of hydrogel mesh, the more release media can be easily contained, thus facilitating drug release [53, 60]. As the temperature increases, the hydrogel mesh gradually shrinks, and less water is contained in the hydrogel shell (Fig. 6a), thus reducing the contact between water and the drug inside the capsule. As the pore size of the hydrogel decreases, the resistance of water and drug release from the capsule to the outside increases, which results in slower drug release. On the other hand, when the temperature decreases, the internal pore size of the hydrogel shell increases, which allows the drug release from the inside of the hydrogel capsule to the outside by diffusion [39, 61]. Temperature is the "transfer switch" for the drug release rate of the core–shell hydrogel capsules, which can slow down drug release at higher temperatures and promote it at lower temperatures. Hydrogel capsules are particularly suitable for loading long-term therapeutic drugs that physicians do not recommend patients to take orally when body temperatures are high [62, 63].

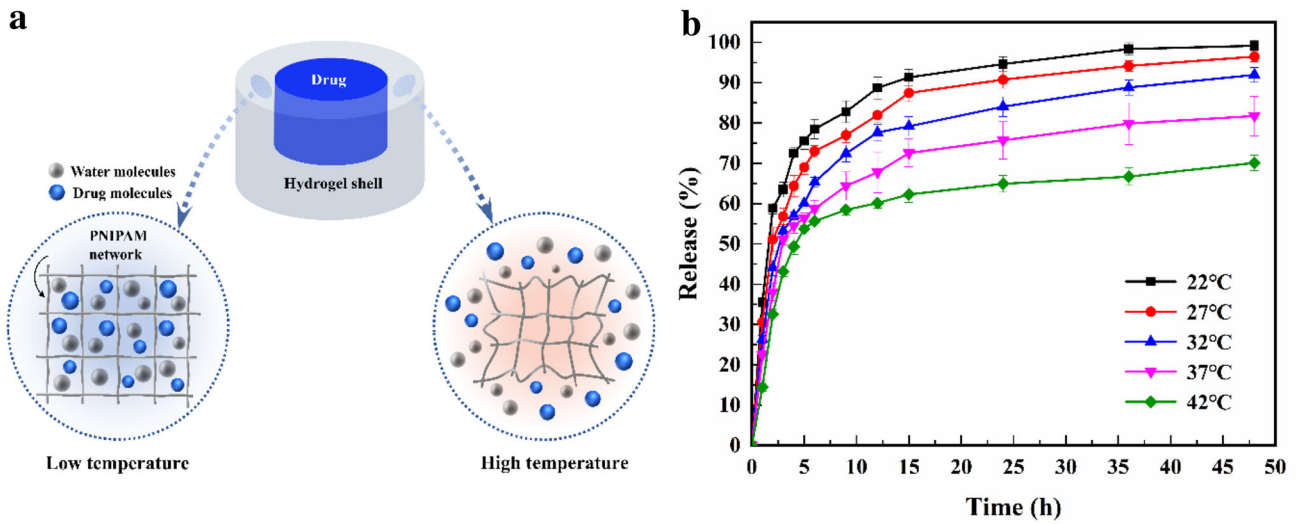

Fig. 6 Effect of temperature on drug release. **a** Schematic diagram of the temperature response of the PNIPAM hydrogel shell. **b** Model drug release profiles of hydrogel capsules with a shell thickness of 2 mm at different temperatures

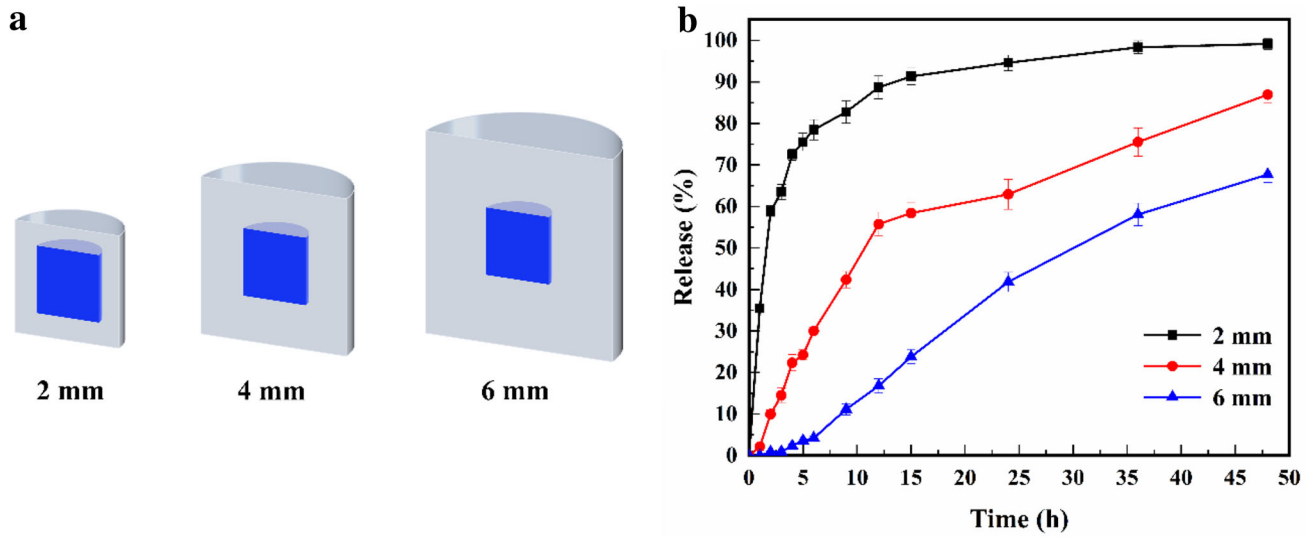

Fig. 7 Effect of shell thickness on drug release. **a** Longitudinal section schematic diagram of hydrogel capsules with different shell thicknesses. **b** Model drug release profiles of hydrogel capsules with different shell thicknesses at 22 °C

Effect of shell thickness on drug release

Figure 7a presents a longitudinal section schematic diagram of hydrogel capsules with different shell thicknesses but the same "core" size. Since UV curing time affects the crosslinking degree and thus the release of drug, in order to make the crosslinking degree of the hydrogel capsules with different thicknesses as similar as possible, capsules with different shell thicknesses were irradiated by UV light for 40 min. The longer UV light irradiation time would allow the NIPAM monomers to cross-link as completely as possible into PNIPAM hydrogel, thus reducing the effect of different crosslinking degrees and for a better comparison of the drug release results. Figure 7b shows the drug release profiles of hydrogel capsules with different shell thicknesses (2, 4, and 6 mm) at 22 °C. After 9 h, approximately 80% of the Brilliant Blue was released from the hydrogel capsule with a shell thickness of 2 mm, while the amounts of drug released from the capsules with shell thicknesses of 4 mm and 6 mm were approximately 42% and 11%, respectively. According to the experimental results, drug release becomes slower as the shell thickness increases. The time it takes for the drug to diffuse through the hydrogel further depends on the diffusion length [58, 61]. Therefore, the shell thickness of the hydrogel capsules affects drug release. The diffusion length extends with the increase of shell thickness of the hydrogel

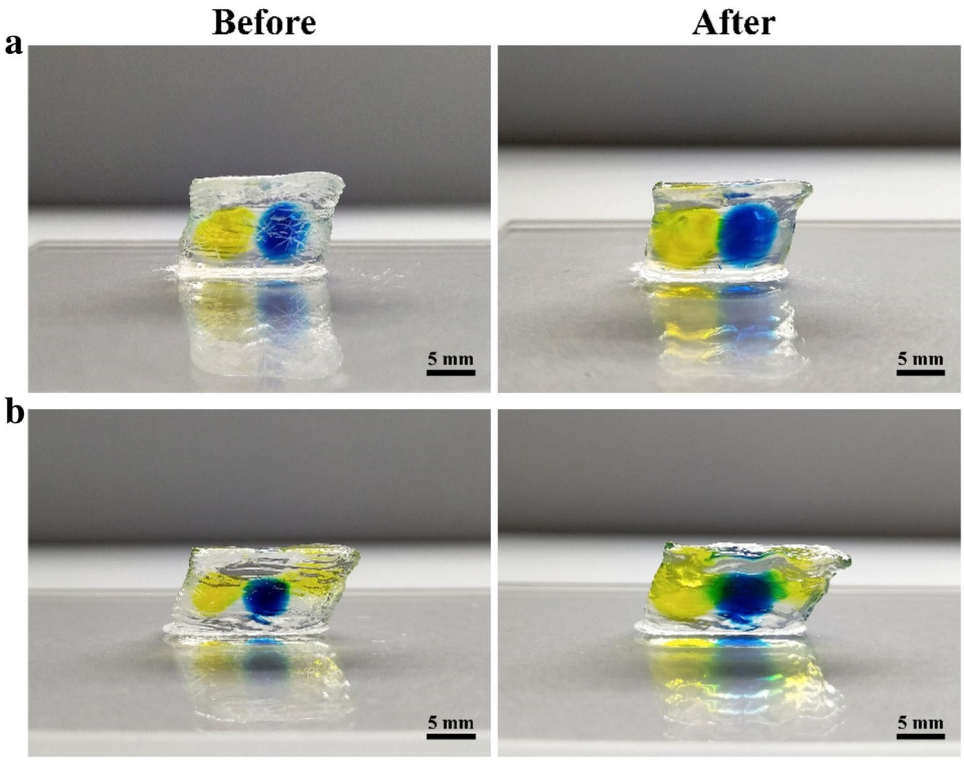

Fig. 8 4D-printed PNIPAM hydrogel "multieffect single capsules". **a** Sample photographs of 4D-printed hydrogel capsules containing multiple drugs before (left) and after (right) UV curing. **b** Sample photographs of 4D-printed hydrogel capsules containing multiple drugs and different doses of a single drug before (left) and after (right) UV curing

capsules, resulting in a slower release rate, and a longer time period required to release the same amount of drug.

It can be seen from these data that, among the factors affecting drug release from the hydrogel capsules, temperature and shell thickness play critical roles. Therefore, we can program the release behavior by designing the shell thickness of the printed capsules.

Design of "multieffect single capsules"

In drug delivery, to treat one or more diseases, patients may need to take a drug multiple times or take multiple drugs at once [6]. However, different patients have different individual needs, and they may need different plasma concentrations for different drugs. According to the foregoing results of the in vitro drug release profiles, it can be seen that the PNIPAM hydrogel capsules can self-change drug release behavior under different temperatures, and the drug release can be programmed by designing the shell thickness of the capsules. Since the rate of drug diffusion through the hydrogel depends on the diffusion length, with the increase of shell thickness of the hydrogel capsules, the drug release becomes slower. As an extension of the above results and for a proof of concept, we designed 4D-printed smart hydrogel capsules containing multiple drugs and different doses of a single drug (Fig. 8); Brilliant Blue and Lemon Yellow were used as the model drugs. The demonstration represents a conceptual design illustrating that the type and dose of drugs can be customized according to the individual needs of patients, and that drug release can be controlled by both the thickness of the hydrogel shell around the drug core and the release temperature of the capsule to achieve release on demand through such "multieffect single capsules."

Conclusions

In summary, we have demonstrated that the multimaterial extrusion-based 4D-printed core–shell hydrogel capsules are capable of self-regulating drug release profiles, and introduced the design of smart hydrogel capsules containing multiple drugs and different doses of a single drug. The results are promising, such as achieving release on demand and fabricating functional "multieffect single capsules." Multimaterial extrusion 4D printing can independently and precisely control the drug type(s), drug dosage, and shell thickness, which are conducive to personalized drug customization. The analysis of the rheological properties of NIPAM printing inks showed that ink with 1% (w/v) carbomer was the most conducive to printing. The PNIPAM hydrogel was demonstrated to have excellent temperature sensitivity, which endows the hydrogel capsules with a high response to environmental stimuli. In vitro, drug release studies of the hydrogel capsules revealed that the capsules can self-change drug release behavior according to ambient temperature, and that drug release can be programmed by

adjusting the shell thickness of the capsules. This demonstration represents a proof of concept illustrating that the combination of 4D printing technology and smart materials can control drug release in a new and unique fashion. In contrast to traditional passive drug release control, the 4D-printed drug capsules introduce an active control method. The presented 4D-printed hydrogel capsules may be more suitable for loading long-term therapeutic drugs that physicians do not recommend patients to take orally when body temperatures are high. These capsules pioneer the paradigm of smart release, with extensive prospects for application in the smart controlled release of drugs and macromolecular active agents.

Supplementary Information The online version contains supplementary material available at https://doi.org/10.1007/s42242-021-00175-y.

Acknowledgements This research was supported by the National Key R&D Program of China (No. 2018YFB1105100).

Author contributions SZ (Shuo Zu) designed the experiments. SZ (Shuo Zu), ZW, ZS, YX, and SZ (Shuang Zhang) performed the experiments. SZ (Shuo Zu) drafted the manuscript. ZZ, QL, and YG helped in writing, reviewing, and editing. ZZ and QL provided funding for this project and supervised the experiments. All authors approved the final manuscript.

Declarations

Conflict of interest The authors declare that there is no conflict of interest.

Ethical approval This article does not contain any studies with human or animal subjects performed by any of the authors.

References

1. Martinez PR, Goyanes A, Basit AW et al (2017) Fabrication of drug-loaded hydrogels with stereolithographic 3D printing. Int J Pharm 532(1):313–317. https://doi.org/10.1016/j.ijpharm.2017.09.003
2. Tan YJN, Yong WP, Kochhar JS et al (2020) On-demand fully customizable drug tablets via 3D printing technology for personalized medicine. J Control Release 322:42–52. https://doi.org/10.1016/j.jconrel.2020.02.046
3. Ilbawi AM, Anderson BO (2015) Cancer in global health: how do prevention and early detection strategies relate? Sci Transl Med 7(278):278cm1. https://doi.org/10.1126/scitranslmed.3008853
4. Alomari M, Mohamed FH, Basit AW et al (2015) Personalised dosing: printing a dose of one's own medicine. Int J Pharm 494(2):568–577. https://doi.org/10.1016/j.ijpharm.2014.12.006
5. Goyanes A, Wang J, Buanz A et al (2015) 3D printing of medicines: engineering novel oral devices with unique design and drug release characteristics. Mol Pharm 12(11):4077–4084. https://doi.org/10.1021/acs.molpharmaceut.5b00510
6. Sun Y, Soh S (2015) Printing tablets with fully customizable release profiles for personalized medicine. Adv Mater 27(47):7847–7853. https://doi.org/10.1002/adma.201504122
7. Hamburg MA, Collins FS (2010) The path to personalized medicine. N Engl J Med 363(4):301–304. https://doi.org/10.1056/NEJMp1006304
8. Wening K, Breitkreutz J (2011) Oral drug delivery in personalized medicine: unmet needs and novel approaches. Int J Pharm 404(1):1–9. https://doi.org/10.1016/j.ijpharm.2010.11.001
9. Mura S, Couvreur P (2012) Nanotheranostics for personalized medicine. Adv Drug Del Rev 64(13):1394–1416. https://doi.org/10.1586/erm.13.15
10. Murphy S, Atala A (2014) 3D bioprinting of tissues and organs. Nat Biotechnol 32(8):773–785. https://doi.org/10.1038/nbt.2958
11. Berman B (2012) 3-D printing: the new industrial revolution. Bus Horiz 55(2):155–162. https://doi.org/10.1016/j.bushor.2011.11.003
12. Ventola CL (2014) Medical applications for 3D printing: current and projected uses. Pharm Ther 39(10):704–711 (PMCID: PMC6139809. PMID: 30228688)
13. Rowe CW, Katstra WE, Palazzolo RD et al (2000) Multimechanism oral dosage forms fabricated by three dimensional printing™. J Control Release 66(1):11–17. https://doi.org/10.1016/s0168-3659(99)00224-2
14. Okwuosa TC, Stefaniak D, Arafat B et al (2016) A lower temperature FDM 3D printing for the manufacture of patient-specific immediate release tablets. Pharm Res 33(11):2704–2712. https://doi.org/10.1007/s11095-016-1995-0
15. Goyanes A, Buanz ABM, Basit AW et al (2014) Fused-filament 3D printing (3DP) for fabrication of tablets. Int J Pharm 476(1):88–92. https://doi.org/10.1016/j.ijpharm.2014.09.044
16. Goyanes A, Chang H, Sedough D et al (2015) Fabrication of controlled-release budesonide tablets via desktop (FDM) 3D printing. Int J Pharm 496(2):414–420. https://doi.org/10.1016/j.ijpharm.2015.10.039
17. Okwuosa TC, Pereira BC, Arafat B et al (2017) Fabricating a shell-core delayed release tablet using dual FDM 3D printing for patient-centred therapy. Pharm Res 34(2):427–437. https://doi.org/10.1007/s11095-016-2073-3
18. Wang J, Goyanes A, Gaisford S et al (2016) Stereolithographic (SLA) 3D printing of oral modified-release dosage forms. Int J Pharm 503(1):207–212. https://doi.org/10.1016/j.ijpharm.2016.03.016
19. Martinez PR, Goyanes A, Basit AW et al (2018) Influence of geometry on the drug release profiles of stereolithographic (SLA) 3D-printed tablets. AAPS PharmSciTech 19(8):3355–3361. https://doi.org/10.1208/s12249-018-1075-3
20. Khaled SA, Burley JC, Alexander MR et al (2014) Desktop 3D printing of controlled release pharmaceutical bilayer tablets. Int J Pharm 461(1–2):105–111. https://doi.org/10.1016/j.ijpharm.2013.11.021
21. Khaled SA, Burley JC, Alexander MR et al (2015) 3D printing of five-in-one dose combination polypill with defined immediate and sustained release profiles. J Control Release 217:308–314. https://doi.org/10.1016/j.jconrel.2015.09.028
22. Fina F, Goyanes A, Gaisford S et al (2017) Selective laser sintering (SLS) 3D printing of medicines. Int J Pharm 529(1):285–293. https://doi.org/10.1016/j.ijpharm.2017.06.082
23. Boehm RD, Miller PR, Daniels J et al (2014) Inkjet printing for pharmaceutical applications. Mater Today 17(5):247–252. https://doi.org/10.1016/j.mattod.2014.04.027
24. Daly R, Harrington TS, Martin GD et al (2015) Inkjet printing for pharmaceutics—a review of research and manufacturing. Int J Pharm 494(2):554–567. https://doi.org/10.1016/j.ijpharm.2015.03.017
25. Dong Y, Wang S, Ke Y et al (2020) 4D printed hydrogels: fabrication, materials, and applications. Adv Mater Technol 5(6):2000034. https://doi.org/10.1002/admt.202000034

26. Alhnan MA, Okwuosa TC, Sadia M et al (2016) Emergence of 3D printed dosage forms: opportunities and challenges. Pharm Res 33(8):1817–1832. https://doi.org/10.1007/s11095-016-1933-1
27. Fan DY, Li Y, Wang X et al (2020) Progressive 3D printing technology and its application in medical materials. Front Pharmacol. https://doi.org/10.3389/fphar.2020.00122
28. Castilho M, Levato R, Bernal PN et al (2021) Hydrogel-based bioinks for cell electrowriting of well-organized living structures with micrometer-scale resolution. Biomacromol 22(2):855–866. https://doi.org/10.1021/acs.biomac.0c01577
29. Ge Q, Dunn C, Qi H et al (2014) Active origami by 4D printing. Smart Mater Struct 23(9):094007. https://doi.org/10.1088/0964-1726/23/9/094007
30. Lee AY, An J, Chua CK (2017) Two-way 4D printing: a review on the reversibility of 3D-printed shape memory materials. Engineering 3(5):663–674. https://doi.org/10.1016/J.ENG.2017.05.014
31. Lee J, Kim HC, Choi JW et al (2017) A review on 3D printed smart devices for 4D printing. Int J Precis Eng Manuf-Green Technol 4(3):373–383. https://doi.org/10.1007/s40684-017-0042-x
32. Hoare TR, Kohane DS (2008) Hydrogels in drug delivery: progress and challenges. Polymer 49(8):1993–2007. https://doi.org/10.1016/j.polymer.2008.01.027
33. Dreiss CA (2020) Hydrogel design strategies for drug delivery. Curr Opin Colloid Interface Sci 48:1–17. https://doi.org/10.1016/j.cocis.2020.02.001
34. Zhang Y, Khademhosseini A (2017) Advances in engineering hydrogels. Science 356(6337):eaaf3627. https://doi.org/10.1126/science.aaf3627
35. Jen AC, Wake MC, Mikos AG (1996) Review: hydrogels for cell immobilization. Biotechnol Bioeng 50(4):357–364. https://doi.org/10.1002/(SICI)1097-0290(19960520)50:4%3c357::AID-BIT2%3e3.0.CO;2-K
36. Gaharwar AK, Peppas NA, Khademhosseini A (2014) Nanocomposite hydrogels for biomedical applications. Biotechnol Bioeng 111(3):441–453. https://doi.org/10.1002/bit.25160
37. Vedadghavami A, Minooei F, Mohammadi MH et al (2017) Manufacturing of hydrogel biomaterials with controlled mechanical properties for tissue engineering applications. Acta Biomater 62:42–63. https://doi.org/10.1016/j.actbio.2017.07.028
38. Lee KY, Mooney DJ (2001) Hydrogels for tissue engineering. Chem Rev 101(7):1869–1880. https://doi.org/10.1021/cr000108x
39. Zhuo RX, Li W (2003) Preparation and characterization of macroporous poly(*N*-isopropylacrylamide) hydrogels for the controlled release of proteins. J Polym Sci Part A Polym Chem 41(1):152–159. https://doi.org/10.1002/pola.10570
40. Li B, Gao Y, Li X et al (2011) Chitosan hydrogels with 3D Liesegang ring structure for rifampicin release. J Control Release 152:e47–e49. https://doi.org/10.1016/j.jconrel.2011.08.114
41. Kim H, Sohn H (2020) Oxidized porous silicon nanoparticles covalent-bonded with levofloxacin in hydrogel polymer as a drug delivery system. J Nanosci Nanotechnol 20(8):4619–4623. https://doi.org/10.1166/jnn.2020.17843
42. Olmos-Juste R, Alonso-Lerma B, Pérez-Jiménez R et al (2021) 3D printed alginate-cellulose nanofibers based patches for local curcumin administration. Carbohydr Polym 264:118026. https://doi.org/10.1016/j.carbpol.2021.118026
43. Croitoru-Sadger T, Yogev S, Shabtay-Orbach A et al (2019) Two-component cross-linkable gels for fabrication of solid oral dosage forms. J Control Release 303:274–280. https://doi.org/10.1016/j.jconrel.2019.04.021
44. Kamlow MA, Vadodaria S, Gholamipour-Shirazi A et al (2021) 3D printing of edible hydrogels containing thiamine and their comparison to cast gels. Food Hydrocoll 116(5):106550. https://doi.org/10.1016/j.foodhyd.2020.106550
45. Haring AP, Tong Y, Halper J et al (2018) Programming of multicomponent temporal release profiles in 3D printed polypills via core-shell, multilayer, and gradient concentration profiles. Adv Healthc Mater 7(16):1800213. https://doi.org/10.1002/adhm.201800213
46. Wang Y, Miao Y, Zhang J et al (2018) Three-dimensional printing of shape memory hydrogels with internal structure for drug delivery. Mater Sci Eng C 84:44–51. https://doi.org/10.1016/j.msec.2017.11.025
47. Han D, Lu ZC, Chester SA et al (2018) Micro 3D printing of a temperature-responsive hydrogel using projection micro-stereolithography. Sci Rep 8(1):1963. https://doi.org/10.1038/s41598-018-20385-2
48. Ziolkowski B, Ates Z, Gallagher S et al (2013) Mechanical properties and UV curing behavior of poly(*N*-isopropylacrylamide) in phosphonium-based ionic liquids. Macromol Chem Phys 214(7):787–796. https://doi.org/10.1002/macp.201200616
49. Lee H, Ko SY, Park JO et al (2014) Fabrication of *N*-isopropylacrylamide (NIPAAM) based micro-hydrogel using UV LED microscope. In: 14th International conference on control, automation and systems. pp 342–344
50. Schild HG (1992) Poly(*N*-isopropylacrylamide):experiment, theory and application. Prog Polym Sci 17(2):163–249. https://doi.org/10.1016/0079-6700(92)90023-R
51. Chen Z, Zhao D, Liu B et al (2019) 3D printing of multifunctional hydrogels. Adv Funct Mater 29(20):1900971. https://doi.org/10.1002/adfm.201900971
52. Chimene D, Lennox KK, Kaunas RR et al (2016) Advanced bioinks for 3D printing: a materials science perspective. Ann Biomed Eng 44(6):2090–2102. https://doi.org/10.1007/s10439-016-1638-y
53. He L, Zuo Q, Xie S et al (2011) Intelligent hydrogels for drug delivery system. Recent Pat Drug Deliv Formul 5(3):265–274. https://doi.org/10.2174/187221111797200533
54. Waalen J, Buxbaum JN (2011) Is older colder or colder older? The association of age with body temperature in 18,630 individuals. J Gerontol A Biol Sci Med Sci 66(5):487–492. https://doi.org/10.1093/gerona/glr001
55. Belezia BF, da Paixão LC, Diniz TR et al (2007) Electrocardiographic manifestations of hypothermia and the "J (Osborn) wave." Crit Care 11(3):P45. https://doi.org/10.1186/cc5832
56. Afrassiabi A, Hoffman AS, Cadwell LA (1987) Effect of temperature on the release rate of biomolecules from thermally reversible hydrogels. J Membr Sci 33(2):191–200. https://doi.org/10.1016/S0376-7388(00)80377-4
57. Huffman A, Afrassiabi A, Dong L (1986) Thermally reversible hydrogels: II. Delivery and selective removal of substances from aqueous solutions. J Control Release 4(3):213–222. https://doi.org/10.1016/0168-3659(86)90005-2
58. Li J, Mooney D (2016) Designing hydrogels for controlled drug delivery. Nat Rev Mater 1(12):16071. https://doi.org/10.1038/natrevmats.2016.71
59. Young ME, Carroad PA, Bell RL (1980) Estimation of diffusion coefficients of proteins. Biotechnol Bioeng 22(5):947–955. https://doi.org/10.1002/bit.260220504
60. Qiu Y, Park K (2001) Environment-sensitive hydrogels for drug delivery. Adv Drug Del Rev 53(3):321–339. https://doi.org/10.1016/s0169-409x(01)00203-4
61. Brazel CS, Peppas NA (2000) Modeling of drug release from swellable polymers. Eur J Pharm Biopharm 49(1):47–58. https://doi.org/10.1016/s0939-6411(99)00058-2
62. Hutchinson A, Olinsky A, Landau L (2010) Long term atropine in chronic severe childhood asthma. Aust Paediatr J 16(4):267–269. https://doi.org/10.1111/j.1440-1754.1980.tb01313.x
63. Xu J, Han QB, Li SL et al (2013) Chemistry, bioactivity and quality control of Dendrobium, a commonly used tonic herb in traditional Chinese medicine. Phytochem Rev 12(2):341–367. https://doi.org/10.1007/s11101-013-9310-8